Available online at www.sciencedirect.com
SCIENCE DIRECT®
Chemical Physics Letters 412 (2005) 190–194
CHEMICAL PHYSICS LETTERS
www.elsevier.com/locate/cplett

Photocurrent spectroscopy of double wall carbon nanotubes

A. Mohite [a], G.U. Sumanasekera [b], K. Hirahara [c], S. Bandow [c], S. Iijima [c], B.W. Alphenaar [a,*]

[a] Department of Electrical and Computer Engineering, University of Louisville, Louisville, KY 40292, USA
[b] Department of Physics, University of Louisville, Louisville, KY 40292, USA
[c] Department of Materials Science and Engineering, 21st Century COE, Meijo University, Nagoya 468-8502, Japan

Received 3 May 2005
Available online 20 July 2005

Abstract

We describe spectroscopy measurements of double wall carbon nanotubes using a displacement photocurrent technique. Peaks in the photocurrent are observed at excitation energies corresponding to the spacing of van Hove singularities for both the inner and outer shells of the nanotube. The shell assignment for the peaks can be made by comparing the spectra before and after the formation of the inner shell. The level spacing observed for the inner shell suggests that the standard tight binding model is insufficient to describe the electron energy spectra for extremely small tubes.

One of the fascinating aspects of single wall nanotube (SWNT) electronics is the clearly observable inter-relationship between nanotube structure and electronic spectra. The variation of the electron density of states with nanotube diameter and chirality has been well documented in both experiment and theory [1]. Multi wall nanotubes (MWNTs) have also received considerable experimental attention, in part because their large size makes them relatively easy to incorporate into electronic devices [2]. The MWNT electronic spectrum is difficult to model, however, since calculations must include a large number of individual shells, together with shell–shell interactions. Recently, techniques for synthesizing double wall nanotubes (DWNTs) have been developed [3–6]. Being the simplest form of multi wall tube, DWNTs provide a tractable system to explore the electron energy spectrum of a multi-shell system. Preliminary experiments on DWNTs have mainly concentrated on describing the vibrational spectra of the inner and outer shells using Raman techniques. There have been few, if any, measurements of the DWNT electron energy spectrum.

Here, we report on photocurrent spectroscopy measurements to determine the electron energy spectrum of DWNTs. We observe peaks in the photocurrent at excitation energies that we relate to the spacing of van Hove singularities in the electron density of states for both the inner and outer shells. The level spacing observed for the outer shell agrees with predictions of the standard zone folding approach applied to tight binding calculations for a graphene sheet. The level spacing associated with the inner shell, however, appears to be influenced by the effects of curvature on neighboring atomic orbitals. Overlap between the inner and outer shell features results in an apparent shift in the outer shell peaks following the formation of the inner shell.

DWNTs are created using the 'peapod' synthesis technique [3], which provides the possibility to study directly the transformation from a SWNT into a DWNT. First, SWNTs are synthesized using high-temperature pulsed laser vaporization of a carbon target containing approximately 1% Fe–Ni. Following acid purification, the SWNTs are heated at 420 °C in dry air to remove

* Corresponding author. Fax: +1 502 852 1577.
E-mail address: brucea@louisville.edu (B.W. Alphenaar).

0009-2614/$ - see front matter © 2005 Elsevier B.V. All rights reserved.
doi:10.1016/j.cplett.2005.06.109

residual amorphous carbon and to open the tube ends. Next, the SWNTs are combined with C_{60} molecules in a sealed ampoule and heated to 400 °C. This results in the diffusion of the C_{60} vapor into the interior of the SWNTs forming 'peapods', or SWNTs containing chains of C_{60} molecules. Finally, the peapods are heated at 1200 °C in vacuum, causing the C_{60} molecules to coalesce into small diameter tubes. The result is a double-shelled tube structure, with the inner shell diameter located around that of the C_{60} molecules and the outer shell diameter defined by the original SWNT. Transmission electron microscopy of the DWNTs synthesized in this way (inset to Fig. 1) shows that they are highly uniform with an average outer shell diameter of 1.4 nm and an average inner shell diameter of 0.7 nm.

Raman scattering spectra were taken of our SWNT and DWNT samples at room temperature in the true backscattering configuration with an incident beam perpendicular to the sample surface using 1064-nm Nd-YAG-excitation. The Raman scattered laser light was analyzed using a FT-Raman spectrometer (BOMEM DA3+) equipped with a holographic notch filter to eliminate the elastically scattered light. Fig. 1 shows the Raman spectra of the SWNT (dashed line) and DWNT (solid line) samples. (The DWNT was formed using the peapod synthesis technique on the SWNT sample, so that the two may be compared directly.) Data are plotted for Raman shifts from 100 to 400 cm^{-1} in the range of the radial breathing modes. For the SWNTs, peaks are observed at $\omega_1(\text{outer}) = 162$ cm^{-1} and $\omega_2(\text{outer}) = 178$ cm^{-1}. The diameter, d, of the outer shell can be estimated from $d = A/\omega_r$, where A is a constant and ω_r is the radial breathing mode frequency. Using a value for $A = 234$ cm^{-1} (averaged from those available in the literature [7]) gives $d_1(\text{outer}) = 1.44$ nm and $d_2(\text{outer}) = 1.32$ nm. After the SWNTs are transformed into DWNTs, two additional peaks appear at $\omega_1(\text{inner}) = 337$ cm^{-1} and $\omega_2(\text{inner}) = 360$ cm^{-1}. The inner diameter radii determined from these peaks are $d_1(\text{inner}) = 0.69$ nm and $d_2(\text{inner}) = 0.65$ nm. The inner and outer shell diameters obtained from the Raman spectra are in good agreement with those obtained from the TEM analysis.

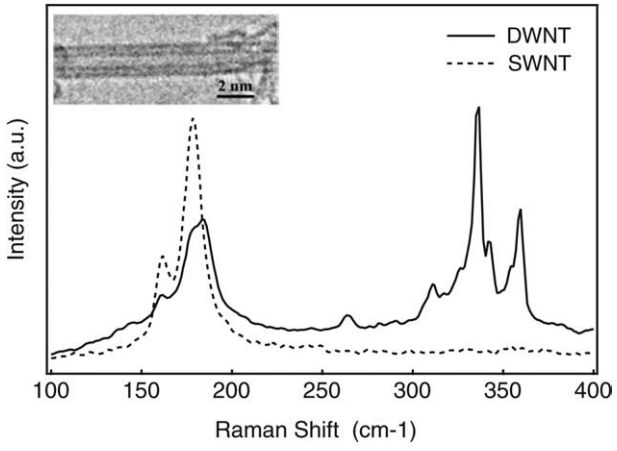

Fig. 1. Room temperature Raman spectra taken for the SWNT (dashed line) and DWNT (solid line) samples for an excitation wavelength of 1064 nm in the range of the radial breathing modes. Inset: TEM image of a typical DWNT.

To probe the electron energy spectrum of the SWNT and DWNT samples, we use a displacement photocurrent spectroscopy technique – the details of which have been recently described [8]. Briefly, a nanotube film is deposited on a glass slide that is anchored to a grounded copper block within an optical access flow cryostat (see Fig. 2a). The nanotubes are coupled to ground capacitively, through the glass dielectric, and coupled to the high side of the circuit by a wire silver-painted to a corner of the film. Pulsed laser light incident on the nanotube film excites charge carriers, which redistribute to create an ac voltage across the nanotube/insulator/metal capacitor. This is measurable as a displacement current from the nanotube film to ground. We illuminate the sample using an optical parametric amplifier (OPA) excited by a pulsed Ti Sapphire regenerative amplifier. The pulse width is 120 fs with a repetition rate of 1 kHz and the photon energy is tunable between 0.4 and 4 eV. The laser power is kept constant at 25 mW. The resulting displacement current is amplified and measured using a lock-in detector.

Fig. 2b shows the displacement photocurrent of a SWNT film measured at 300 K and with a dc bias of 10 V. A series of peaks are observed as a function of incident photon energy, the lowest three having energies of 0.62, 1.39, and 1.85 eV, along with at least two additional peaks at higher excitation energies. Similar peaks have been observed in absorbance measurements of SWNT films and have been attributed to excitation across van Hove singularities in the electron energy spectrum [9,10] (or more recently, to the formation of excitons [11,12]). The standard approach to determine the nanotube electron energy spectrum is zone-folding of the tight binding calculated dispersion for a graphene sheet (ZF-TB model) [13]. This method ignores the influence of curvature on the carbon–carbon bonds, but is thought to be accurate for large diameter tubes. Fig. 3a shows predictions of the ZF-TB model for the separation of the lowest three energy transitions (S11, S22, and M11) in the nanotube density of states, for all possible nanotubes with diameters ranging from 1.2 to 1.55 nm. (We do not consider the higher energy transitions, because there is considerable overlap in the transition energies in this regime, making mapping to the data difficult.) We also plot the positions of the three lowest energy SWNT photocurrent peaks (solid circle, square, and diamond) assuming a diameter of 1.48 nm (the average of the two diameters obtained from the Raman data). It is seen that the peaks in the SWNT displacement current spectrum are in good agreement with the ZF-TB model. Recent work has suggested that

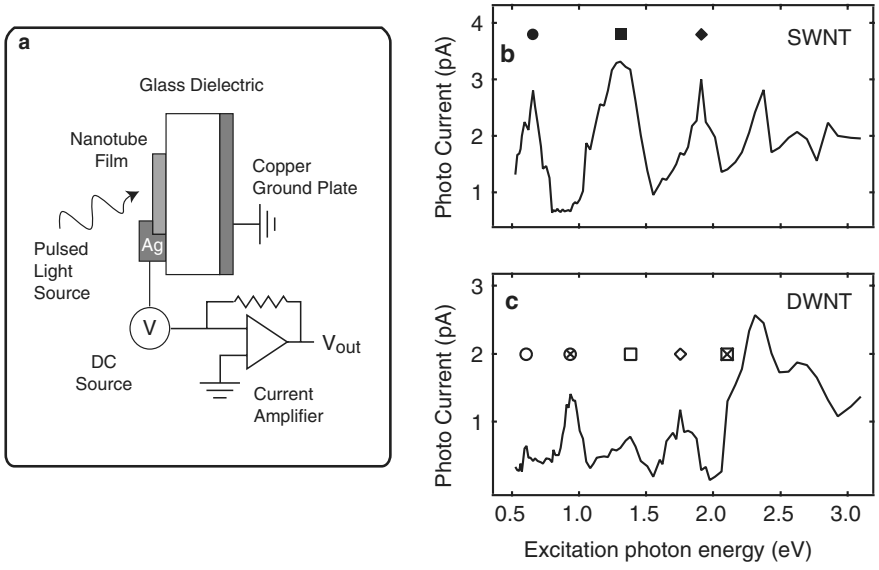

Fig. 2. (a) Diagram illustrating the displacement photocurrent measurement technique. (b) SWNT displacement photocurrent spectrum. The lowest three energy peaks are assigned to the S11 (●), S22 (■), and M11(◆) transitions. (c) DWNT displacement photocurrent spectrum. Peaks are assigned to the S11 (○), S22 (□), and M11 (◇) outer shell transitions, and to the S11 (⊗) and S22 (⊠) inner shell transitions.

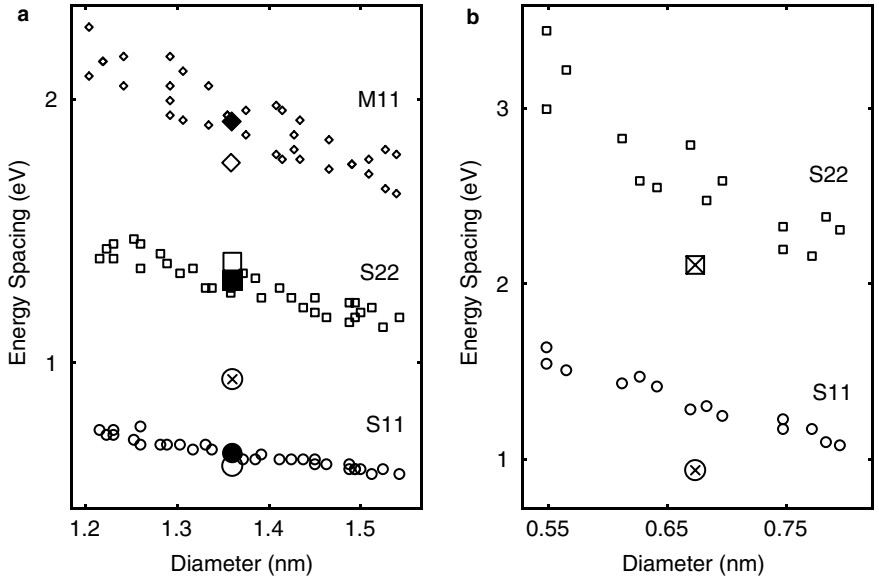

Fig. 3. (a) Comparison of the photocurrent peak energies with calculated gap energies. Gap energies are calculated for the S11(○), S22 (□), and M11 (◇) transitions for all nanotubes with diameters between 1.2 and 1.55 nm using the ZF-TB model assuming a overlap integral constant of 3.1. The measured photocurrent peak energies for a diameter of 1.36 nm are shown for the SWNT (large solid symbols) and DWNT (large open symbols). The position of the S11 transition for the inner shell is also indicated (crossed circle). (b) Comparison of the ZF-TB model with experiment for nanotube diameters between 0.54 and 0.81 nm. The positions of the peaks assigned to the inner shell are plotted for a diameter of 0.67 nm (crossed symbols).

exciton binding energies in carbon nanotubes are extremely high, making excitons, rather than interband transitions, the primary photoexcitations in semiconducting SWNTs [11,12]. The agreement of our data with the simple ZF-TB model implies however, that it is unnecessary to invoke excitons to explain our results.

The displacement photocurrent spectrum for the DWNT sample is shown in Fig. 2c. The three peaks originally associated with the S11, S22, and M11 transition of the outer nanotube shell are once again observed, although there is a small energy shift in the position of the peaks from the SWNT values, and the relative amplitude of the peaks has changed. Two higher energy peaks are also observed. These match the position of peaks observed in the SWNT results, suggesting that they are due to transitions in the outer shell electron

energy spectrum. The most striking difference between the SWNT and DWNT results is the appearance of a new peak in the DWNT energy spectrum at 0.94 eV. As can be seen in Fig. 3a, this new peak lies between the S11 and S22 transitions for the outer shell and is thus thought to correspond to a transition within the inner shell electron energy spectrum. Fig. 3b shows ZF-TB predictions for the S11 transition energy in the neighborhood of the inner shell diameter (0.54–0.81 nm). The observed S11 inner shell transition energy is plotted in Fig. 3b for a diameter of 0.67 nm (the average diameter determined from the Raman data). It can be seen that the ZF-TB model substantially overestimates the observed energy of the S11 transition. For diameters less than 1 nm, the ZF-TB model fails because the carbon–carbon bonds on the curved nanotube surface can no longer be considered equivalent [14–16]. The influence of curvature has been accounted for in the literature using a variety of different models. In Table 1, we compare predictions from three of these models [15,17,18], along with the ZF-TB result. We choose the nanotube among those studied in the models whose diameter is closest to the diameter of the inner shell. As seen in Table 1, the models including curvature all predict transition energies that are substantially closer to our experiment than the ZF-TB model. Kane et al. [18], who derive their result using the π-electron two-dimensional Dirac Hamiltonian, provides the best approximation to our results.

Given that the peak at 0.94 eV is due to the S11 transition for the inner tube, we also expect to see evidence for the S22 inner tube transition. The only available prediction for the energy of the S22 transition comes from the ZFT-TB model, which we already know provides too large of value for the S11 inner tube transition energy. However, if we assume that the error between experiment and the ZFT-TB model is the same for the S22 transition as for the S11 transition, we expect to observe the S22 inner tube peak at an energy of 2.1 eV (as shown in Fig. 3b). This is very close to one of the higher energy peaks, but there does appear to be an extra feature in the DWNT photocurrent near 2.1 eV (as shown in Fig. 2c) that we can tentatively ascribe to the S22 inner tube transition.

Table 1
Experimentally determined energy spacing for the S11 transition compared with the results of the ZF-TB model, and three models that include the influence of curvature on the nanotube electron state distribution

	(n, m)	Diameter (nm)	ΔE (eV)
Photocurrent		0.67	0.94
ZF-TB	(6, 4)	0.686	1.30
[15]	(10, 0)	0.78	0.85
[17]	(6, 4)	0.686	1.09
[18]	(6, 4)	0.686	0.98

A remaining issue is how the interaction between the outer and inner shells influences the DWNT electron energy spectrum. As noted, we do observe a shift in the transition energies for the outer shell DWNT peaks compared with the SWNT peaks. This is particularly noticeable for the M11 transition, which shifts by 0.16 eV. One possibility is that this shift is due to shell–shell interactions. Although a model for this interaction is not available, the narrow linewidth of the Raman peak for the inner tube (compared with the SWNT data) suggests that the interaction strength is relatively weak. Furthermore, in a recent experiment [19], Raman peaks associated with the outer shell were found to be strongly modified by Br doping, while the peaks associated with the inner shell were unchanged, suggesting a lack of shell–shell interaction. Another possibility is that overlap of the peaks due to the outer and inner shells results in an apparent shift. For example, overlap of the M11 outer shell transition with the S22 inner shell transition could account for the observed shift in the outer shell transition energy.

In conclusion, we have used Raman spectroscopy and displacement photocurrent spectroscopy to probe the vibrational and electron energy spectrum of DWNTs. From the Raman data, we are able to determine the diameter of the inner and outer shells of the DWNT and use this information to help identify the observed features in the electron energy spectrum. Features associated with the inner shell can be accounted for, provided that the curvature of the small diameter inner shell is included. Our results confirm that the curvature of the nanotube influences the distribution of nanotube electron states for sufficiently small diameter tubes.

Acknowledgements

The authors thank Lie Liu for providing the code for the energy calculations, G. Chen and P.C. Eklund for assistance with the Raman spectroscopy, and R.W. Cohn and J. Kielkopf for useful discussions. Funding provided by NSF (No. ECS–0224114) and NASA (No. NCC 5-571).

References

[1] M. Dresselhaus, G. Dresselhaus, Ph. Avouris (Eds.), Carbon Nanotubes: Synthesis, Structure, Properties and Applications, Springer, Berlin, 2001.
[2] C. Schonenberger, A. Bachtold, C. Strunk, J.P. Salvetat, L. Forro, Appl. Phys. A 69 (1999) 283.
[3] S. Bandow, T. Hiraoka, T. Yumura, K. Hirahara, H. Shinohara, S. Iijima, Chem. Phys. Lett. 337 (2001) 348.
[4] J.L. Hutchison, N.A. Kiselev, E.P. Krinichnaya, A.V. Krestinin, R.O. Loutfy, A.P. Morawsky, V.E. Muradyan, E.D. Obraztsova, J. Sloan, S.V. Terekhov, D.N. Zakharov, Carbon 39 (2001) 63.

[5] L.J. Ci, Z.L. Rao, Z.P. Zhou, D.S. Tang, Y.Q. Yan, Y.X. Liang, D.F. Liu, H.J. Yuan, W.Y. Zhou, G. Wang, W. Liu, S.S. Xie, Chem. Phys. Lett. 359 (2002) 63.
[6] W.C. Ren, F. Li, J.A. Chen, S. Bai, H.M. Cheng, Chem. Phys. Lett. 359 (2002) 196.
[7] S. Bandow, G. Chen, G.U. Sumansekera, R. Gupta, M. Yudasaka, S. Iijima, P.C. Eklund, Phys. Rev. B 66 (2002) 075416.
[8] A. Mohite, S. Chakraborty, P. Gopinath, G.U. Sumanasekera, B.W. Alphenaar, Appl. Phys. Lett. 86 (2005) 061114.
[9] M.E. Itkis, S. Niyogi, M.E. Meng, M.A. Hamon, H. Hu, R.C. Haddon, Nano Lett. 2 (2002) 155.
[10] H. Kataura, Y. Kumazawa, Y. Maniwa, I. Umezu, S. Suzuki, Y. Ohtsuka, Y. Achiba, Synth. Met. 103 (1999) 2555.
[11] O.J. Korovyanko, C.-X. Sheng, Z.V. Vardeny, A.B. Dalton, R.H. Baughman, Phys. Rev. Lett. 92 (2004) 17403.
[12] C.D. Spataru, S. Ismail-Beigi, L.X. Benedict, S.G. Louie, Phys. Rev. Lett. 92 (2004) 77402.
[13] R. Saito, M. Fujita, G. Dresselhaus, M.S. Dresselhaus, Appl. Phys. Lett. 60 (1992) 2204.
[14] N. Hamada, S.I. Sawada, A. Oshiyama, Phys. Rev. Lett. 68 (1992) 1579.
[15] H. Yorikawa, S. Muramatsu, Phys. Rev. B 52 (1995) A2723.
[16] K. Hirahara, S. Bandow, H. Kataura, M. Kociak, S. Iijima, Phys. Rev. B 70 (2004) 205422.
[17] V. Zolyomi, J. Kurti, Phys. Rev. B 70 (2004) 085403.
[18] C.L. Kane, E.J. Mele, Phys. Rev. Lett. 78 (1997) 1932.
[19] G. Chen, S. Bandow, E.R. Margine, C. Nisoli, A.N. Kolmogorov, V.H. Crespi, R. Gupta, G.U. Sumansekera, S. Iijima, P.C. Eklund, Phys. Rev. Lett. 90 (2003) 257403.